Synthesis, Structural Characterization, and Readsorption Behavior of a Solid Solution Aluminum Phosphite/Ethylenediphosphonate Series

Howard G. Harvey,[†] Jerry Hu,[‡] and Martin P. Attfield*[,†,§]

Davy−Faraday Research Laboratory, The Royal Institution of Great Britain, 21 Albemarle Street, London, W1S 4BS, UK, Materials Research Laboratory, University of California, Santa Barbara, California 93106, and School of Crystallography, Birkbeck College, Malet Street, London, WC1E 7HX, UK

Received July 17, 2002. Revised Manuscript Received September 20, 2002

Members of the new solid solution aluminum phosphite/ ethylenediphosphonate series, $Al_2[(O_3PC_2H_4PO_3)_{1-x}(HPO_3)_{2x}](H_2O)_2F_2{\cdot}H_2O$ ($0 \le x \le 0.32$), have been prepared and fully characterized. The full dehydration behavior of the parent material of this series, $Al_2[O_3PC_2H_4PO_3](H_2O)_2F_2{\cdot}H_2O$ ($x = 0$) has been resolved. On heating the material to 230 °C the extraframework water is the primary species desorbed and the framework structure remains intact as determined from the crystal structure of the partially dehydrated material, $Al_2[O_3PC_2H_4PO_3](H_2O)_2F_2{\cdot}0.51(3)H_2O$. Above 150 °C, but more noticeably above 200 °C, framework water is lost, resulting in the formation of 4- and 5-coordinated Al centers. By 340 °C all the framework water and some fluorine is lost resulting in the collapse of the crystalline material. The phosphite substituted materials ($0 < x \le 0.32$) are shown, by diffraction and spectroscopic techniques, to be single-phase solid solutions. Rietveld refinement of the structure of the $x = 0.19$ member reveals that a random substitution of phosphite groups for diphosphonate species exists throughout the bulk of the material and that the remainder of the framework remains unaltered by incorporation of this moiety. The readsorption behavior of the materials ($0 \le x \le 0.32$) indicates that the temperature at which the extraframework water is first removed decreases as x increases and that the amount of water lost and degree of readsorption increase as x increases. These results indicate that the porosity of the materials can be controlled in a manner conducive to their rational design.

Introduction

The area of inorganic−organic hybrid materials is a rapidly expanding field of materials chemistry that possesses vast potential regarding the design of novel materials with specific structure and functionality. One such group of hybrid materials that has received considerable interest in recent years is the metal phosphonate/diphosphonate family which has great possibilities for application in the areas of sorption and ion-exchange,[1−3] sensing,[4,5] charge storage,[6] and catalysis.[7,8]

Early work focused primarily on utilizing phosphonic acids for the synthesis of new materials, but this has been extended to include the use of diphosphonic acids [$(HO)_2OPRPO(OH)_2$], where R is an organic group) that have proved to be versatile building units for the synthesis of extended open framework materials. The diphosphonate group is involved in framework connection with the organic portion acting as a controllable spacer or pillar, and the two inorganic $-PO_3$ groups chelating the metal ions to form one-,[9] two-,[10] and, most frequently, three-dimensional structures.[11,12] Careful selection of the R group allows the interlamellar distance, or pore size, and potentially the shape-selective properties within the resulting structure to be controlled. Metal diphosphonates containing various metal cations that have been synthesized include those of the alkaline earth,[13] transition,[14−17] rare earth,[18] and more recently, the Group 13 metals, Al and Ga.[19,20]

* To whom correspondence should be addressed. Tel: 44-20-7631-6813. Fax: 44-20-7631-6803. E-mail: m.attfield@mail.cryst.bbk.ac.uk.
[†] Davy−Faraday Research Laboratory.
[‡] University of California, Santa Barbara.
[§] Birkbeck College.

(1) Maeda, K.; Kiyozumi, Y.; Mizukami, F. *J. Phys. Chem. B* **1997**, *101*, 4402.
(2) Odobel, F.; Bujoli, B.; Massiot, D. *Chem. Mater.* **2001**, *13*, 163.
(3) Sharma, C. V. K.; Clearfield, A. *J. Am. Chem. Soc.* **2000**, *122*, 4394.
(4) Alberti, G.; Casciola, M.; Costantino, U.; Peraio, A.; Montoneri, E. *Solid State Ionics* **1992**, *50*, 315.
(5) Alberti, G.; Casciola, M. *Solid State Ionics* **1997**, *97*, 177.
(6) Vermeulen, L. A.; Thompson, M. E. *Nature* **1992**, *358*, 656.
(7) Deniaud, D.; Schollorn, B.; Mansuy, D.; Rouxel, J.; Battioni, P.; Bujoli, B. *Chem. Mater.* **1995**, *7*, 995.
(8) Maillet, C.; Janvier, P.; Pipelier, M.; Praveen, T.; Andres, Y.; Bujoli, B. *Chem. Mater.* **2001**, *13*, 2879.
(9) Zheng, L. M.; Song, H. H.; Duan, C. Y.; Xin, X. Q. *Inorg. Chem.* **1999**, *38*, 5061.
(10) Gao, Q. M.; Guillou, N.; Nogues, M.; Cheetham, A. K.; Ferey, G. *Chem. Mater.* **1999**, *11*, 2937.
(11) Serre, C.; Ferey, G. *Inorg. Chem.* **1999**, *38*, 5370.
(12) Distler, A.; Sevov, S. C. *Chem. Commun.* **1998**, *15*, 959.
(13) Poojary, D. M.; Zhang, B. L.; Clearfield, A. *An. Quim.-Int. Ed.* **1998**, *94*, 401.
(14) Poojary, D. M.; Zhang, B. L.; Clearfield, A. *J. Am. Chem. Soc.* **1997**, *119*, 12550.
(15) Poojary, D. M.; Zhang, B. L.; Clearfield, A. *Chem. Mater.* **1999**, *11*, 421.
(16) RiouCavellec, M.; Serre, C.; Robino, J.; Nogues, M.; Greneche, J. M.; Ferey, G. *J. Solid State Chem.* **1999**, *147*, 122.
(17) Barthelet, K.; Riou, D.; Ferey, G. *Solid State Sci.* **2001**, *3*, 203.

10.1021/cm0212663 CCC: $25.00
Published on Web 11/26/2002

Many of the framework metal diphosphonates contain channels, the dimensions of which are determined by the length of the organic R group and the interpillar spacing. The interpillar spacings reported for diphosphonate materials are typically narrower (<5 Å) than that desired for the numerous applications requiring easy access to the internal volume of the materials. Thus, methods to increase, and control, the distance between the diphosphonate pillars and the porosity of the material have been pursued vigorously. The majority of work has been performed on tetravalent and divalent metal cation diphosphonate materials for which three methods to increase the interpillar separation have been reported. The first method, reported by Dines et al.,[21] involves pillaring the host material γ-zirconium phosphate with a phosphate ester, $(HO)_2OPOR'OPO(OH)_2$, and a diphosphonic acid $(HO)_2OPRPO(OH)_2$ (R′ is shorter than R by two CH_2 units) of similar dimensions. Porosity was incorporated within the resultant material, $Zr(O_3PO(CH_2)_6OPO_3)_{0.5}(O_3P(CH_2)_8PO_3)_{0.5}$, through hydrolysis of the phosphate ester in the material to yield smaller P−OH groups. The second method involves the controlled topotactic substitution of a diphosphonate material within a layered host, for example the anionic substitution of $[(HO)O_2PRPO_2(OH)]^{2-}$ for $H_2PO_4^-$ ions in the γ-zirconium phosphate phase, $ZrPO_4(H_2PO_4)\cdot 2H_2O$.[22] The final common method involves formation of the porous material by coprecipitation of a metal species with the diphosphonic acid and a smaller spacer substituent X-$PO(OH)_2$, such as phosphoric acid (X = OH), phosphorous acid (X = H), or methylphosphonic acid (X = CH_3). This methodology has been used to form several microporous diphosphonate materials, of which $Zr(HPO_3)_{1.2}(O_3PRPO_3)_{0.4}$ (R = 3, 3′, 5, 5′- tetramethylbiphenyl) and the zinc arylenediphosphonate/phosphate system are most noticeable for the novel synthetic strategy used to design the former, and the inclusion of a divalent metal cation in the latter.[23−25] The coprecipitation method has also been used to yield several mixed derivatives of tetravalent and divalent metal phosphonates that are either single-phase solid solutions or staged structures.[26,27] However, the coprecipitation technique is not always successful for these phosphonate materials, as evidenced by attempts to incorporate the phosphite group into the microporous aluminum methylphosphonate, AlMePO-β.[28]

All the materials hitherto described have been shown to have greater porosity than their respective unsubstituted parent materials; however, as far as the authors are aware, the crystallinity of all the reported materials has been too low to yield any of their structures by full crystallographic analysis. Hitherto, only visual inspection of diffraction patterns, computer modelling, spectroscopic, and gas adsorption methods have been used to deduce structural models for these materials.[24,25]

We recently reported the synthesis and structure of the first aluminum diphosphonate material, $Al_2[O_3PC_2H_4PO_3](H_2O)_2F_2\cdot H_2O$, a framework structure containing a one-dimensional channel system with one crystallographic species of extraframework molecule occupying the channels.[19] The structural changes that $Al_2[O_3PC_2H_4PO_3](H_2O)_2F_2\cdot H_2O$ undergoes as it loses its extraframework and framework water molecules are reported herein, as determined by the use of spectroscopic and crystallographic methods. These results are used to explain the properties of the first mixed-derivative solid solution trivalent metal phosphite/diphosphonate series, $Al_2[(O_3PC_2H_4PO_3)_{1-x}(HPO_3)_{2x}](H_2O)_2F_2\cdot H_2O$ ($0 \le x \le 0.32$) for which we describe the synthesis, characterization, and readsorption behavior in this work. The crystal structure of one member of the series is described, as determined by Rietveld analysis of synchrotron X-ray diffraction data, and represents the first crystal structure determination for this class of mixed-derivative diphosphonate material.

Experimental Section

Materials and Methods. All reagents and solvents were obtained from Aldrich, with the exception of phosphorous acid (Alfa) and ethylenediphosphonic acid (Lancaster), and were used without further purification.

Fourier transform infrared (FTIR) spectra were collected on pellets pressed from ground mixtures of the samples with KBr using a Perkin-Elmer 1725X spectrometer.

Magic angle spinning solid-state nuclear magnetic resonance (MAS SS NMR) ^{27}Al spectra were recorded on a Bruker DMX 500 spectrometer at 11.7 T using a 4-mm probe and referenced to $Al(NO_3)_3$. Acquisition times of 5 ms were used with 13 kHz spinning speeds, and relaxation delays of 1 s. ^{31}P MAS SS NMR spectra were recorded using a Bruker MSL 300 spectrometer. An 85% solution of H_3PO_4 was used as the reference with the spectrometer operating at a frequency of 121.495 MHz, a sample spinning speed of 6.3 kHz, and recycle delays of 30 s. A sample spinning speed of 7.066 kHz was used for the $x = 0$ sample.

Thermogravimetric analysis (TGA) data were collected on a Mettler Toledo SDTA841E thermal analysis unit coupled to a Pfeiffer Thermostar 0-300 molecular mass spectrometer with the sample being heated under nitrogen from 25 to 950 °C at a heating rate of 5 °C min^{-1}. Readsorptive thermogravimetric analyses were performed using a Seiko instrument EXSTAR 6000 thermogravimetric analyzer. Water readsorption experiments were conducted using 10 mg of sample and the following heating program for all materials: (i) hold at ambient temperature for 10 min; (ii) heat to 135 °C at 2 °C min^{-1}; (iii) hold at 135 °C for 30 min; (iv) cool to ambient temperature at 2 °C min^{-1}; and (v) hold at ambient temperature for 20 min. Steps (i)−(iii) and (v) were conducted under dry helium; for step (iv) the helium gas input stream was routed through a water bubbler. For one substituted sample, steps (ii)−(iv) were repeated. The helium flow gas was passed through the device at a flow rate of 100 mL min^{-1} for all experiments.

X-ray thermodiffraction was performed at the Materials Science Laboratory, Daresbury. The experimental setup comprises a FR571 Enraf Nonius rotating anode X-ray generator ($CuK\alpha_1$) used in conjunction with a high-temperature furnace and an INEL position-sensitive detector. Diffraction patterns

(18) Serpaggi, F.; Ferey, G. *Microporous Mesoporous Mater.* **1999**, *32*, 311.
(19) Harvey, H. G.; Teat, S. J.; Attfield, M. P. *J. Mater. Chem.* **2000**, *10*, 2632.
(20) Bujoli-Doeuff, M.; Evain, M.; Janvier, P.; Massiot, D.; Clearfield, A.; Gan, Z. H.; Bujoli, B. *Inorg. Chem.* **2001**, *40*, 6694.
(21) Dines, M. B.; Cooksey, R. E.; Griffith, P. C.; Lane, R. H. *Inorg. Chem.* **1983**, *22*, 1004.
(22) Alberti, G.; Marmottini, F.; Murciamascaros, S.; Vivani, R. *Angew. Chem., Int. Ed. Engl.* **1994**, *33*, 1594.
(23) Alberti, G.; Costantino, U.; Marmotti, F.; Vivani, R.; Zappelli, P. *Angew. Chem., Int. Ed. Engl.* **1993**, *32*, 1357.
(24) Alberti, G.; Costantino, U.; Marmottini, F.; Vivani, R.; Zapelli, P. *Microporous Mesoporous Mater.* **1998**, *21*, 297.
(25) Zhang, B. L.; Poojary, D. M.; Clearfield, A. *Inorg. Chem.* **1998**, *37*, 1844.
(26) Scott, K. J.; Zhang, Y.; Wang, R. C.; Clearfield, A. *Chem. Mater.* **1995**, *7*, 1095.
(27) Clearfield, A.; Wang, J. D.; Tian, Y.; Stein, E.; Bhardwaj, J. *J. Solid State Chem.* **1995**, *117*, 275.
(28) Hix, G. B.; Carter, V. J.; Wragg, D. S.; Morris, R. E.; Wright, P. A. *J. Mater. Chem.* **1999**, *9*, 179.

Table 1. Initial Synthesis Gel Compositions and Product Formulas of $Al_2[(O_3PC_2H_4PO_3)_{1-x}(HPO_3)_{2x}](H_2O)_2F_2{\cdot}H_2O$

$H_3PO_3/H_2O_3PC_2H_4PO_3H_2/Al_2(SO_4)_3{\cdot}18H_2O/HF^a$/Pyridine^b/$H_2O$	$Al[(O_3PC_2H_4PO_3)_{1-x}(HPO_3)_{2x}](H_2O)_2F_2{\cdot}H_2O^c$
0:2.16:1:8.65:54.6:144	$Al_2[O_3PC_2H_4PO_3](H_2O)_2F_2{\cdot}(H_2O)$
2.16:1.08:1:8.65:54.6:144	$Al_2[(O_3PC_2H_4PO_3)_{0.81}(H_3PO_3)_{0.39}](H_2O)_2F_2{\cdot}H_2O$
2.88:0.72:1:8.65:54.6:144	$Al_2[(O_3PC_2H_4PO_3)_{0.68}(H_3PO_3)_{0.64}](H_2O)_2F_2{\cdot}H_2O$

[a] HF/pyridine (70 wt % HF). [b] Includes pyridine from HF/pyridine. [c] Formulas obtained from ^{31}P MAS SS NMR data.

Table 2. Crystal Data and Structure Refinement Parameters for $Al_2[O_3PC_2H_4PO_3](H_2O)_2F_2{\cdot}0.51(3)H_2O$

formula	$Al_2[O_3PC_2H_4PO_3](H_2O)_2F_2{\cdot}0.51(3)H_2O$
formula weight	323.098
temperature (K)	123
wavelength (Å)	0.6931
crystal system	monoclinic
space group	$P2_1/m$
a (Å)	4.938(1)
b (Å)	12.060(3)
c (Å)	8.186(1)
β (°)	92.045(4)
V (Å^3)	487.2(2)
Z	2
D_C (g/cm^3)	2.202
μ (mm^{-1})	0.692
crystal size (mm)	0.050 × 0.040 × 0.005
θ range for data collection	2.43−25.69°
index ranges	$-6 \le h \le 6$, $-15 \le k \le 15$, $-10 \le l \le 10$
reflections collected	4111
independent reflections	1042
refinement method	full-matrix least-squares on F^2
data/restraints/parameters	1042/0/93
goodness-of-fit on F^2	0.991
R_{int}	0.0782
$R1$ [$I > 2\sigma(I)$], $R1$ (all data)	0.0886, 0.1227
$wR2$ [$I > 2\sigma(I)$], $wR2$ (all data)	0.2164, 0.2356
$\Delta\rho_{max}/\Delta\rho_{min}$ (e Å^{-3})	1.940, −0.668

were collected at 4 °C intervals. Room-temperature X-ray diffraction patterns were collected using a Siemens D500 diffractometer employing Ge-monochromated CuKα_1 radiation.

Sample Preparation. $Al_2[O_3PC_2H_4PO_3](H_2O)_2F_2{\cdot}H_2O$ was synthesized as microcrystals following the method described previously.[19] The dehydrated form of the above material, $Al_2[O_3PC_2H_4PO_3](H_2O)_2F_2{\cdot}yH_2O$, was synthesized by heating a sample of single crystals of $Al_2[O_3PC_2H_4PO_3](H_2O)_2F_2{\cdot}H_2O$ in a tube furnace under flowing nitrogen at 220 °C for 3 h. The crystals were heated and cooled at 0.5 °C min^{-1} to prevent fracturing of the crystals. Samples were prepared for the ^{27}Al MAS SS NMR experiments by heating a series of $Al_2[O_3PC_2H_4PO_3](H_2O)_2F_2{\cdot}H_2O$ starting materials to temperatures in the range from 50 to 400 °C, at 50 °C intervals, with each sample being held at the desired temperature for 3 h.

The solid-solution series of materials $Al_2[(O_3PC_2H_4PO_3)_{1-x}(H_3PO_3)_{2x}](H_2O)_2F_2{\cdot}H_2O$ were prepared following a method similar to that described previously,[19] with a fraction of the ethylenediphosphonic acid replaced by phosphorous acid during the initial mixing of the gel. The compositions of initial synthetic mixtures are summarized in Table 1. The ratio of phosphorous acid to diphosphonate in the synthesis gel was adjusted to 2:1 and 4:1 while keeping the total molar amount of phosphorus constant. The products were formed as polycrystalline materials that were filtered, washed with distilled water then acetone, and dried at room temperature.

Single-Crystal Structure Determination. A suitable crystal of $Al_2[O_3PC_2H_4PO_3](H_2O)_2F_2{\cdot}yH_2O$ was attached to a glass fiber and mounted on a Bruker AXS SMART three-circle diffractometer equipped with a CCD area-detector at the microcrystal diffraction facility at Station 9.8 of the SRS, Daresbury, UK. A hemisphere of data was collected with X-ray radiation of wavelength 0.6931 Å, selected using a Si(111) crystal monochromator. Data were collected from a twinned crystal that was indexed using the unit cell parameters found for the fully hydrated material.[19] An empirical absorption correction was applied to the data using the SADABS program.[29] The structure was solved and refined using SHELXTL.[30] The Al, P, C, F, and framework O atoms were found from the initial structure solution with the remaining extraframework O, and H atoms located from difference Fourier maps. The final cycle of full-matrix least-squares refinement included the positional parameters of all atoms, anisotropic thermal parameters of all non-hydrogen atoms, and the occupancy of the extraframework O atom, O(6). The isotropic thermal parameters of the hydrogen atoms were fixed at sensible values. The final reliability values were $R(F) = 0.0884$ and $R_w(F^2) = 0.2164$. These residuals are higher than usual because the data set could not be de-twinned and some reflections had a contribution to their intensity from other twins. The crystal data and details of data collection are summarized in Table 2. The fractional atomic coordinates, occupancies, equivalent isotropic thermal factors, and selected bond lengths and angles are provided in the Supporting Information.

Table 3. Crystal Data and Structure Refinement Parameters for $Al_2[(O_3PC_2H_4PO_3)_{0.810(5)}(HPO_3)_{0.38(1)}](H_2O)_2F_2{\cdot}H_2O$

formula	$Al_2[(O_3PC_2H_4PO_3)_{0.810(5)}(HPO_3)_{0.38(1)}](H_2O)_2F_2{\cdot}H_2O$
formula weight	326.529
temperature (K)	298
wavelength (Å)	1.25042
space group	$P2_1/m$
a (Å)	4.97546(3)
b (Å)	11.98967(6)
c (Å)	8.18047(6)
β (°)	92.416(1)
V (Å^3)	487.565(5)
Z	2
D_C (g/cm^3)	2.257
no. of unique reflections	812
no. of fitted parameters	46
R_p	0.0506
R_{wp}	0.0651
R_F	0.0540
χ^2	2.77

Reitveld Structure Refinement. Powder synchrotron X-ray diffraction data were collected on a sample of $Al_2[(O_3PC_2H_4PO_3)_{1-x}(H_3PO_3)_{2x}](H_2O)_2F_2{\cdot}H_2O$ ($x = 0.19$) contained in a 0.5-mm diameter Lindemann glass capillary tube and mounted on the high-resolution powder X-ray diffractometer at station 2.3, SRS, Daresbury. The incident X-ray wavelength was 1.2504 Å, selected using a Si(111) monochromator. Data were collected in increments of 0.01° 2θ from 5 to 25° for 4 s per step, from 25 to 50° for 7 s per step, and from 50 to 90° for 11 s per step.

A Le Bail profile fit was performed initially on the data using the unit cell parameters and symmetry of $Al_2[O_3PC_2H_4PO_3](H_2O)_2F_2{\cdot}H_2O$. [31] The absence of any additional reflections revealed that there was no lowering of symmetry or staging with the incorporation of the phosphite group in the material. A pseudo-Voigt function was selected to describe the peak profile with additional terms used to account for anisotropic particle-size and strain-broadening effects. The background

(29) Siemens Industrial Automation, I. SADABS: Area-Detector Absorption Correction; Madison, WI, 1996.

(30) Sheldrick, G. M. SHELXL-97, Program for Crystal Structure Determination; University of Cambridge: U. K., 1997.

(31) Le Bail, A.; Duroy, H.; Fourquet, J. *Mater. Res. Bull.* **1988**, *23*, 447.

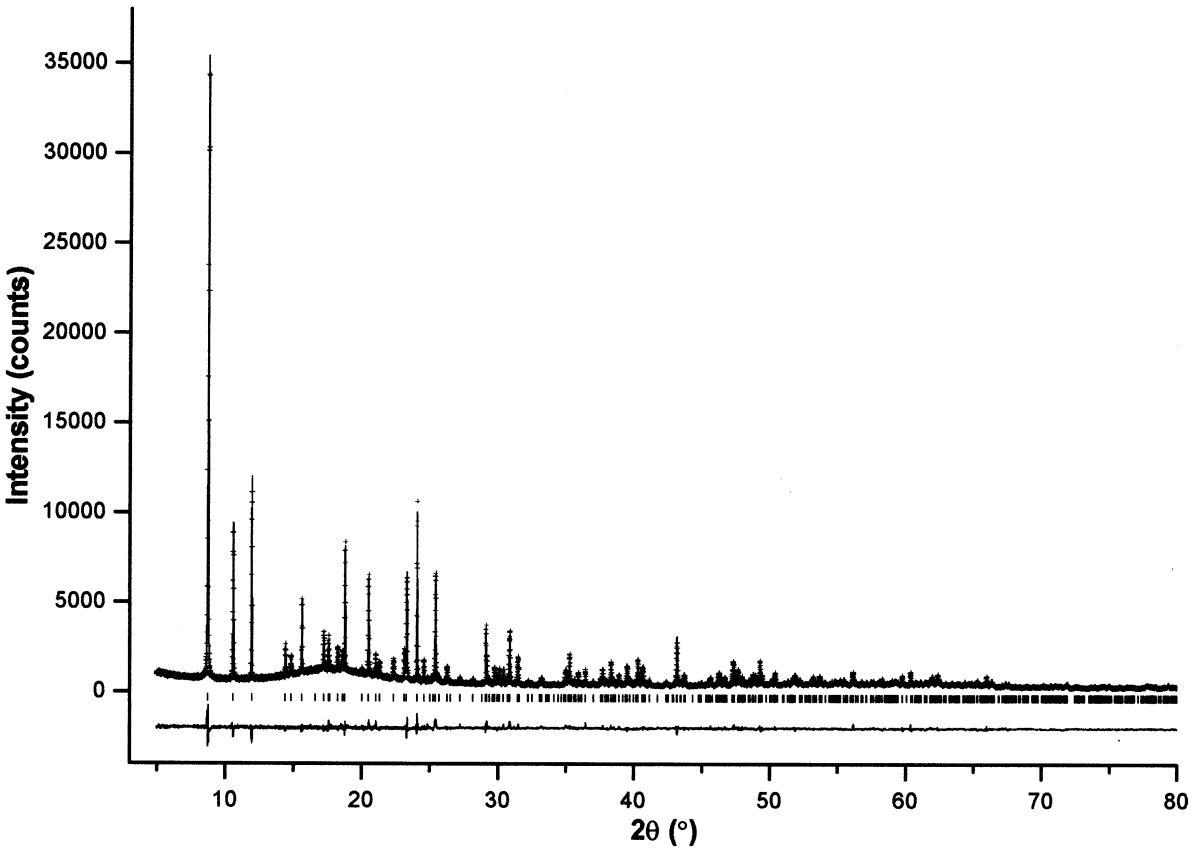

Figure 1. Final observed (crosses), calculated (line), and difference plots for the Rietveld refinement of $Al_2[(O_3PC_2H_4PO_3)_{0.810(5)}(HPO_3)_{0.38(1)}](H_2O)_2F_2{\cdot}H_2O$. The tick marks are calculated 2θ angles for the Bragg peaks.

Table 4. Atomic Coordinates and Isotropic Thermal Parameters (Å^2) for $Al_2[(O_3PC_2H_4PO_3)_{0.810(5)}(HPO_3)_{0.38(1)}](H_2O)_2F_2{\cdot}H_2O$

atom	*x*	*y*	*z*	U_{iso}	occupancy
Al(1)	0.2468(7)	0.25	0.1438(4)	0.0108(3)	1
Al(2)	0.5	0.5	0	0.0108(3)	1
P(1)	0.0088(4)	0.4850(1)	0.2330(2)	0.0108(3)	1
O(1)	0.7206(7)	0.5206(3)	0.1913(4)	0.0091(4)	1
O(2)	0.0410(8)	0.3566(3)	0.2337(5)	0.0091(4)	1
O(3)	0.2065(7)	0.5451(3)	0.1222(5)	0.0091(4)	1
O(4)	0.509(1)	0.25	0.3286(7)	0.0091(4)	1
O(5)	0.007(1)	0.25	0.9481(7)	0.0091(4)	1
O(6)	0.439(1)	0.25	0.6581(7)	0.0091(4)	1
C(1)	0.089(2)	0.5332(6)	0.4428(9)	0.0091(4)	0.810(5)
F(1)	0.4540(7)	0.3516(2)	0.0487(4)	0.0091(4)	1

was fitted using a five-term Cosine Fourier series running through 67 fixed points in the profile. The $Al_2[O_3PC_2H_4PO_3](H_2O)_2F_2{\cdot}H_2O$ structure was used as the initial model for the Rietveld refinement in space group $P2_1/m$.[19] The final cycle of least-squares refinement consisted of 46 terms including the histogram scale factor, detector zero-point error, background coefficients, unit cell parameters, peak shape terms, positional and isotropic thermal parameters for all atoms, and the occupancy of the carbon atom (C(1)) of the diphosphonate group. The isotropic thermal parameters of the Al and P atoms were constrained to have the same value, as were those of the O, F, and C atoms. The crystallographic data are summarized in Table 3. The final observed, calculated, and difference profiles are shown in Figure 1. Final atomic coordinates, isotropic thermal parameters and occupancies are given in Table 4, and selected bond distances and angles are provided in the Supporting Information. The GSAS suite of programs was used for the Le Bail extraction and Rietveld refinement.[32]

Results and Discussion

Dehydration Behavior of $Al_2[O_3PC_2H_4PO_3](H_2O)_2F_2{\cdot}H_2O$. The results of the combined thermal gravimetric analysis (TGA)/molecular mass spectrometry (MMS) analysis of $Al_2[O_3PC_2H_4PO_3](H_2O)_2F_2{\cdot}H_2O$ are shown in Figure 2. As the material is heated the first mass loss of 16.55% occurs between 120 and 330 °C which corresponds to the mass loss expected for the removal of all the extraframework and framework water (calculated, 16.27%). The first derivative of the TGA profile and the profile of the 18 amu (H_2O) loss from the mass spectrometer highlight the fact that this mass loss occurs over a wider temperature range (100−450 °C) and that it occurs in two stages, with the first stage reaching its most rapid rate of loss at 210 °C and the second stage occurring at 285 °C. It is also evident that a clear cutoff does not exist between these two stages of water loss. The first water loss is attributed to the removal of extraframework water species, and the second is associated with removal of the framework water coordinated to the aluminum centers in the structure. The second weight loss in the TGA profile occurs between 600 and 650 °C. This is observed with corresponding peaks in the mass spectrometer profile (see Supporting Information) at 14 (CH_2) and 28 (C_2H_4), 18 (H_2O) and 20 (HF), which corresponds to the degradation of the organic components and evolution of HF and H_2O in this temperature range.

The thermodiffraction behavior of the material is shown in Figure 3. Above 170 °C, minor changes in the diffraction patterns are seen which include the (100) and (200) Bragg peaks at 11.12 and 13.37° 2θ moving to

(32) Von Dreele, R. B.; Larson, A. C. GSAS, General Structure Analysis System; Regents of the University of California: LANSCE, Los Alamos National Laboratory: New Mexico, 1995.

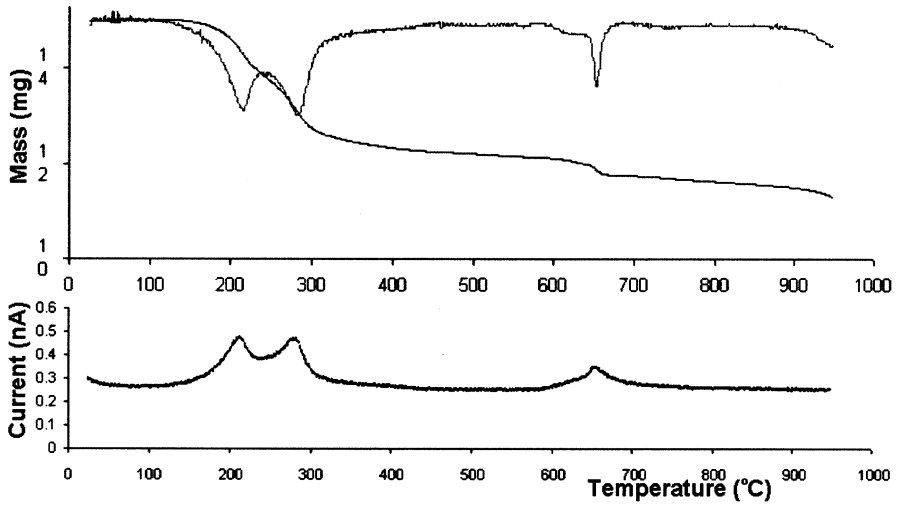

Figure 2. TGA and first derivative curves (top) and mass spectrometry plot (bottom) at 18 amu for $Al_2[O_3PC_2H_4PO_3](H_2O)_2F_2 \cdot H_2O$.

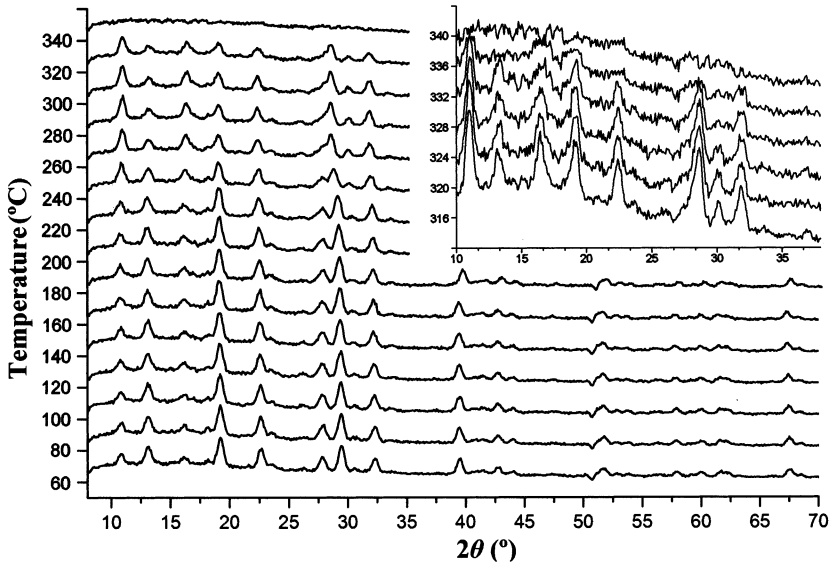

Figure 3. X-ray thermodiffraction pattern of $Al_2[O_3PC_2H_4PO_3](H_2O)_2F_2 \cdot H_2O$. The inset shows the temperature region over which the major loss of crystallinity of the material occurs.

higher angles indicating a decrease in the *a* axis of the unit cell and other minor shifts of peak positions and changes in intensity. A loss of crystallinity is observed between 320 and 336 °C, (inset Figure 3) with the sample becoming amorphous at 340 °C. The temperature range of this loss of crystallinity is correlated to the second water loss, as shown in the TGA/ MMS results.

To determine the actual structure of the material during the temperature range of the two-stage water loss the crystal structure and coordination of the aluminum centers were probed. To confirm that the extraframework water is removed first upon heating and to test the stability of $Al_2[O_3PC_2H_4PO_3](H_2O)_2F_2 \cdot H_2O$ to the loss of extraframework water, a full structural analysis of a dehydrated sample was performed. The structure of $Al_2[O_3PC_2H_4PO_3](H_2O)_2F_2 \cdot 0.51(3)H_2O$ is shown in Figure 4 and is similar to that of the fully hydrated form.[19] The structure is formed from chains of corner-sharing AlO_4F_2 octahedra running parallel to the *b* axis. These chains contain two types of AlO_4F_2 octahedra. The first type contains aluminum, Al(2), coordinated to two fluorine atoms (F(1)) in a trans configuration with the other corners of the octahedron being occupied by four of the oxygen atoms of the diphosphonate groups (O(1) and O(3)). The second octahedron consists of a central aluminum atom, Al(1), bound to the two fluorine atoms (F(1)) in a cis fashion with the other two equatorial positions being occupied by two diphosphonate oxygen atoms (O(2)) and the axial positions filled by coordinated water molecules, O(4) and O(5). The diphosphonate groups link the chains together along the *a*-axis through Al−O−P−O−Al bridges and along the *c*-direction through the ethylene groups to form a framework structure with channels running along the *a*-axis. All the bond distances in this structure are similar to those found in the fully hydrated structure and other materials.[19,33] The remaining extraframework water, O(6), is again located in the same site as that found for the fully hydrated structure, with a partial occupancy of 0.26(2), that corresponds to 51(3)% of the extraframework water being present. This extraframework water implies the crystals were not fully dehy-

(33) Simon, N.; Guillou, N.; Loiseau, T.; Taulelle, F.; Ferey, G. *J. Solid State Chem.* **1999**, *147*, 92.

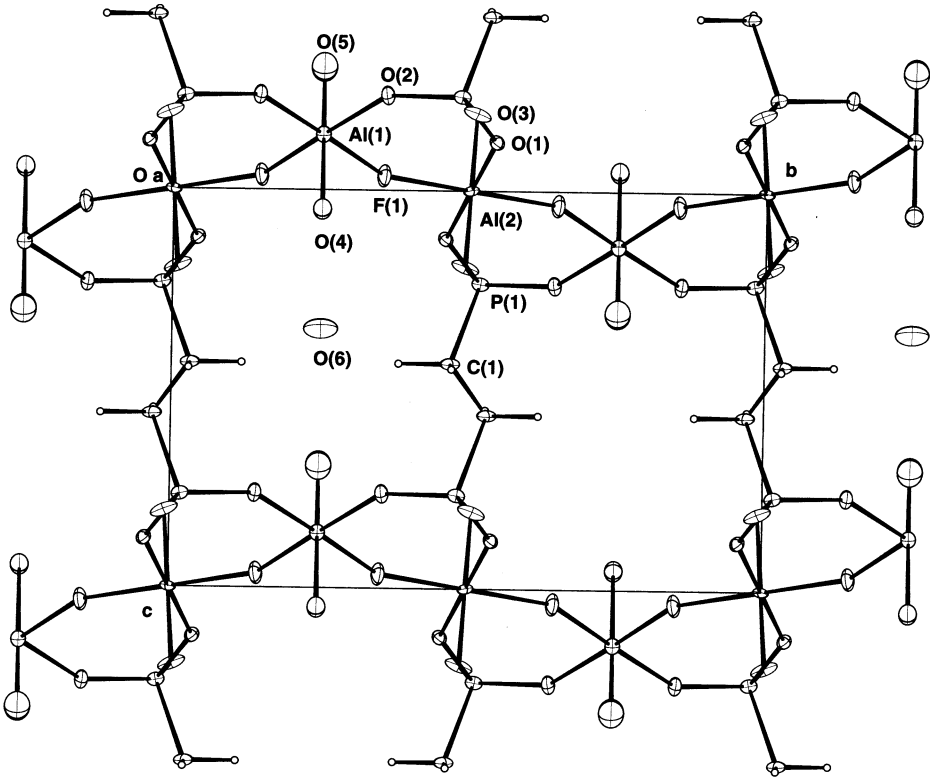

Figure 4. Crystal structure of $Al_2[O_3PC_2H_4PO_3](H_2O)_2F_2 \cdot 0.51(3)H_2O$ viewed along the *a* axis, showing 50% of the extraframework waters. Thermal ellipsoids are shown at 50% probability.

drated during the heating procedure or that slow water readsorption occurred before the data collection was performed. However, the structure refinement shows that the framework of this material is stable with respect to the removal of the extraframework water. The unit cell of the hydrated material shrinks slightly in response to the removal of extraframework water, contracting from 488.9(2) to 487.2(2) $Å^3$ with the largest contraction occurring along the *a* axis; the hydrated form has dimension 4.978(3) Å that reduces to 4.938(1) Å, in agreement with the thermodiffraction results described previously.

The ^{27}Al MAS SS NMR spectra of samples of $Al_2[O_3PC_2H_4PO_3](H_2O)_2F_2 \cdot H_2O$ heated to temperatures in the range 50−400 °C are shown in Figure 5. The room temperature to 150 °C spectra are all similar with one peak at −18 ppm, and its associated spinning sidebands at −109 and 86 ppm, consistent with ^{27}Al in an octahedral environment as reported for aluminophosphates.[34] On increasing the temperature to 200 °C an additional peak at 41 ppm is observed, corresponding to Al in a 4-coordinate environment. [35] This suggests that the beginnings of a structural change of the framework occurs between 150 and 200 °C. At higher temperatures the proportion of 4-coordinated Al increases, with this environment becoming the dominant configuration at temperatures greater than 300 °C. At temperatures ≥250 °C an additional peak is observed at 10 ppm, which is attributed to 5-coordinate aluminum, that increases in intensity as the temperature is increased to 400 °C.[35] The 5-coordinated Al corresponds

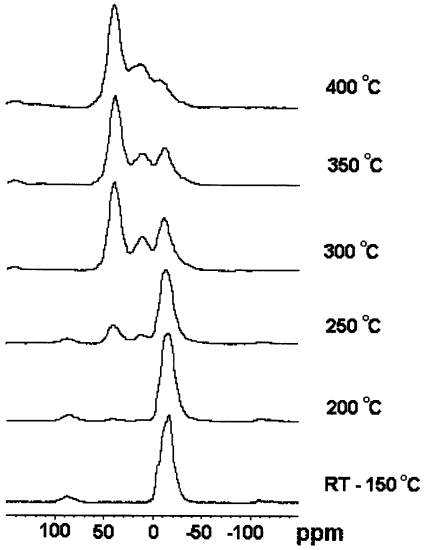

Figure 5. ^{27}Al MAS SS NMR spectra of $Al_2[O_3PC_2H_4PO_3](H_2O)_2F_2 \cdot H_2O$ after heating to the temperatures indicated on the plot.

to some of the Al(1) sites that may have lost only one water molecule or possibly Al(2) sites that have some of the diphosphonate oxygen atoms or fluoride ions removed from the coordination sphere.

This combination of techniques has allowed the full dehydration behavior of $Al_2[O_3PC_2H_4PO_3](H_2O)_2F_2 \cdot H_2O$ to be determined. From 100 to 200 °C the extraframework water is the predominant species to be removed and the framework structure of the material remains intact and stable to loss of the extraframework water. Above 150 °C, but more noticeably above 200 °C, the framework water is lost causing the formation of 4- and 5-coordinated Al centers which are assumed to be

(34) Zahedi-Niaki, M. H.; Xu, G.; Meyer, H.; Fyfe, C. A.; Kaliaguine, S. *Microporous Mesoporous Mater.* **1999**, *32*, 241.
(35) Marichal, C.; Vidal, L.; Delmotte, L.; Patarin, J. *Microporous Mesoporous Mater.* **2000**, *34*, 149.

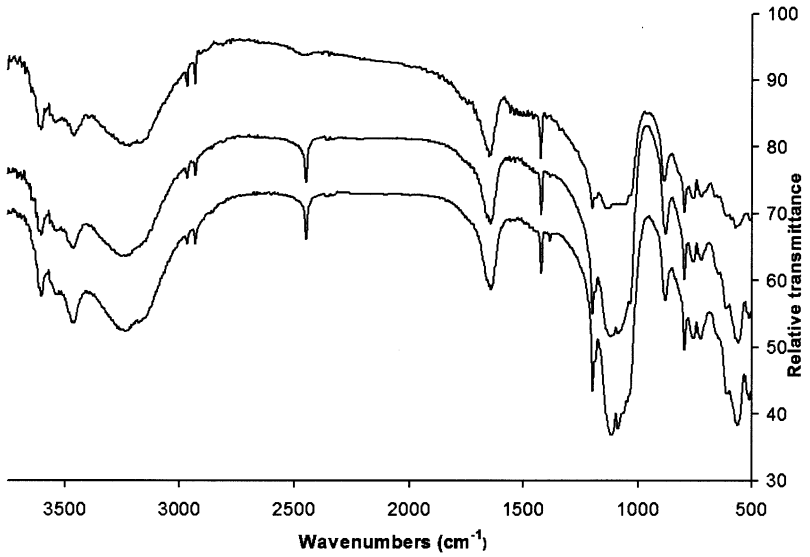

Figure 6. FTIR spectra of $Al_2[(O_3PC_2H_4PO_3)_{1-x}(HPO_3)_{2x}](H_2O)_2F_2{\cdot}H_2O$ for $x = 0$ (top), $x = 0.19$ (middle), and $x = 0.32$ (bottom).

predominantly those formed at Al(1) which has two coordinated water molecules in its primary coordination sphere. As the temperature is increased to 350 °C then more of the Al sites become 4- and 5-coordinated as all the framework water and some fluorine are lost from the system leading to the collapse of the crystalline material by 350 °C. The structure therefore appears to be stable to the loss of the extraframework water O(6), however a structural collapse occurs upon the removal of the majority of the water coordinated to the aluminum, O(4/5). This means that the reversible adsorption properties and microporous nature of the material can be probed only at temperatures low enough (<200 °C) for the majority of water loss to be from the extraframework water.

Synthesis and Characterization of the Solid Solution Aluminum Phosphite/ Ethylenediphosphonate Series: $Al_2[(O_3PC_2H_4PO_3)_{1-x}(HPO_3)_{2x}](H_2O)_2F_2{\cdot}H_2O$ ($0 \leq x \leq 0.32$). The incorporation of phosphorous acid (H_3PO_3) into the initial synthesis gel in varying quantities at the expense of ethylenediphosphonic acid led to the formation of polycrystalline materials. The ratio of the initial synthesis mixtures used are given in Table 1, and when compared to the resultant formulas obtained using other techniques indicate that approximately half of the phosphorous acid incorporated into the gel was incorporated into the solid product. The amount of phosphite incorporated into the product compared to the amount used in the gel indicates that the limit of diphosphonate group substitution is likely to be 50%.

The incorporation of the phosphite group within the substituted materials was confirmed using FTIR spectroscopy. Figure 6, shows the FTIR spectra of the phosphite-substituted materials and the parent compound, $Al_2[O_3PC_2H_4PO_3](H_2O)_2F_2{\cdot}H_2O$, $x = 0$. The peak at 2449 cm^{-1} is attributed to the P−H stretching vibration of the phosphite group, which is observed for the phosphite-substituted materials and is absent in the spectra of the parent compound.[36] The presence of one sharp band and its consistent position in the phosphite-substituted samples indicate that there is a single species present in the two samples. The remainder of each of the spectra of the phosphite-substituted spectra

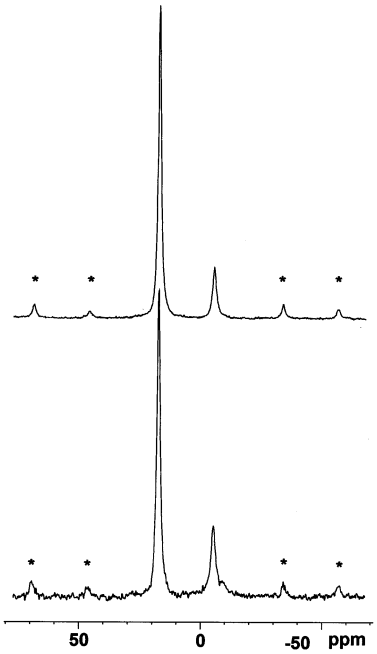

Figure 7. ^{31}P MAS SS NMR spectra of $Al_2[(O_3PC_2H_4PO_3)_{1-x}(HPO_3)_{2x}](H_2O)_2F_2{\cdot}H_2O$: $x = 0.19$ (top) and $x = 0.32$ (bottom). The spinning sidebands are denoted by asterisks (*).

and that of the parent material share the same features which is indicative of there being only one phase present and not a physical mixture of phosphite and diphosphonate phases.

^{31}P MAS SS NMR was used to show the presence of the phosphite group in the substituted materials and to obtain a more quantative estimate of the phosphite content by comparing the ratio of the intensities of the peak, with associated spinning sidebands, of the P nuclei of the phosphite and disphosphonate groups. Figure 7 shows the ^{31}P MAS SS NMR spectra for the two phosphite-substituted materials. The spectra of the phosphite-substituted materials are identical in terms

(36) Dines, M. B.; Digiacomo, P. M.; Callahan, K. P.; Griffith, P. C.; Lane, R. H.; Cooksey, R. E. *Chemically Modified Surfaces in Catalysis and Electrocatalysis*; ACS Symposium Series Vol. 192; American Chemical Society: Washington, DC, 1982.

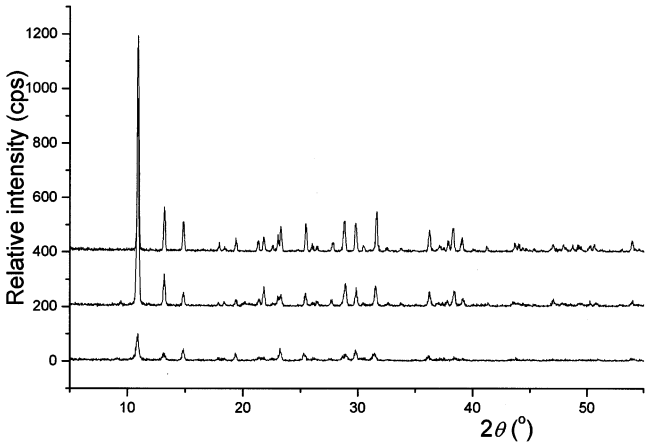

Figure 8. Powder X-ray diffraction patterns of $Al_2[(O_3PC_2H_4PO_3)_{1-x}(HPO_3)_{2x}](H_2O)_2F_2 \cdot H_2O$: $x = 0$ (top), $x = 0.19$ (middle), and $x = 0.32$ (bottom).

of chemical shifts and number of environments present, again indicating that the materials are monophasic. The resonance due to the ^{31}P nuclei of the diphosphonate group is centered at 17.38 ppm, and those due to the ^{31}P nuclei of the phosphite group are centered at −5.32 ppm.[26] The ^{31}P MAS SS NMR spectra for the parent material contains a single peak at 17.38 ppm (see Supporting Information). The formulas of the materials derived from these ratios are given in Table 1.

The powder X-ray diffraction patterns of the materials are shown in Figure 8, and show that the substituted materials are phase pure and their structures are based upon that of the parent framework structure. The unsubstituted $x = 0$ and the $x = 0.19$ phosphite-substituted material are of similar crystallinity. However, the greater degree of phosphite-substitution in the $x = 0.32$ material results in a loss of crystallinity as found in other substituted systems.[25,24]

The $x = 0.19$ phosphite-substituted sample was selected for a full Rietveld analysis (using synchrotron radiation) on the basis of its phosphite content and high crystallinity. Such a refinement has not been performed on any other substituted diphosphonate frameworks of this kind, presumably because of the crystallinity being too low for previously synthesized systems. The incorporated phosphite groups possess the same geometry as the PO_3 groups of the diphosphonate linkages so the presence of additional atomic sites due to the phosphite PO_3 species were not expected to be found in the structure. This was found to be the case, as no indications of split atomic sites or excessive residual electron density were found in the difference Fourier maps at the conclusion of the refinement. The incorporation of the phosphite group into the material manifests itself in the structure refinement through either a decrease in occupancy of the ethylene group of the diphosphonate pillar or the location of the partially occupied site for the hydrogen atom of the phosphite moiety. However, as hydrogen is a poor X-ray scatterer, the former method of refining the occupancy of the C(1) atom of the diphosphonate group provides the only method to determine the degree of phosphite-substitution in the material. The results of the refinement were obtained by refining the occupancy of C(1), $C(1)_{occ}$, and constraining all the isotropic thermal factors of the O, F, and C atoms to have the same value. The final residuals for this refinement were $\chi^2 = 2.77$, $R_{wp} = 6.51$, $R_p = 5.06$, and $R_F^2 = 8.90$, and sensible values of bond lengths and angles were obtained without the use of soft restraints. The resulting value of $C(1)_{occ}$ was 0.810(5) giving a composition of $Al_2[(O_3PC_2H_4PO_3)_{0.810(5)}(HPO_3)_{0.38(1)}](H_2O)_2F_2 \cdot H_2O$, $x = 0.190(5)$, for this phosphite-substituted phase. Several other refinement strategies were performed to validate this result. When the value of $C(1)_{occ}$ was held at unity and all the isotropic thermal factors of the O, F, and C atoms were constrained to have the same value a poorer final fit was obtained with significantly higher final residuals ($\chi^2 = 3.08$, $R_{wp} = 6.87$, $R_p = 5.31$, and $R_F^2 = 9.69$) and an unacceptable range of bond lengths and angles. Next, a similar refinement was performed with $C(1)_{occ} = 1$, and the isotropic thermal factor of C(1), $C(1)_{Uiso}$, was allowed to refine freely. This again resulted in a poorer fit to the reported refinement results with higher final residuals ($\chi^2 = 2.99$, $R_{wp} = 6.77$, $R_p = 5.24$, and $R_F^2 = 9.49$), an unacceptable range of bond lengths and angles, and a very large value for $C(1)_{Uiso} = 0.054(3)$ Å^2. The large magnitude of the $C(1)_{Uiso}$ value suggests that too much electron density was assigned to the C(1) atom and that an occupancy of unity was too high. A final refinement was performed in which $C(1)_{occ}$ and $C(1)_{Uiso}$ were allowed to refine freely which produced final results of quality similar to those reported, with residuals of $\chi^2 = 2.77$, $R_{wp} = 6.52$, $R_p = 5.06$, and $R_F^2 = 8.91$, sensible values

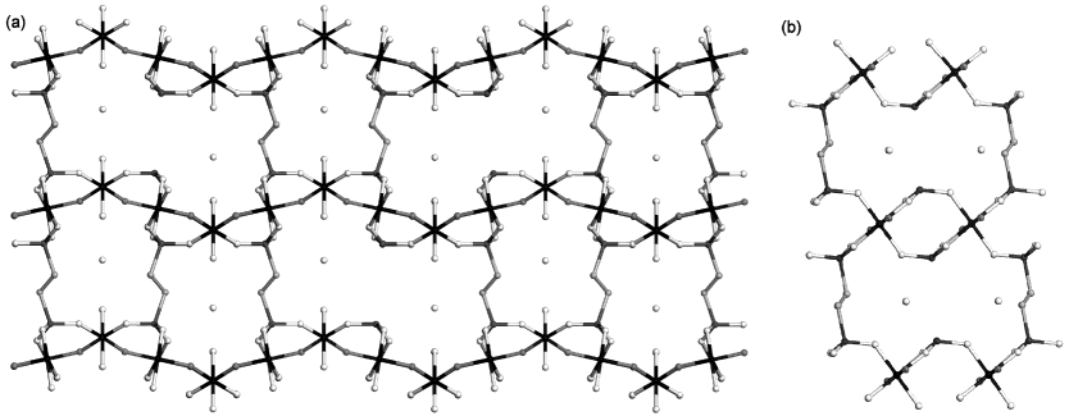

Figure 9. Structure of $Al_2[O_3PC_2H_4PO_3]_{0.810(5)}[H_3PO_3]_{0.38(1)}(H_2O)_2F_2 \cdot H_2O$ viewed (a) along the *a* axis and (b) along the *b* axis. The diphosphonate groups are replaced in a random fashion by phosphite species in proportions close to those given in the formula. The atoms in order of decreasing gray-scale, from black to white, are Al, P, F, C, and O. H atoms are omitted from the structure.

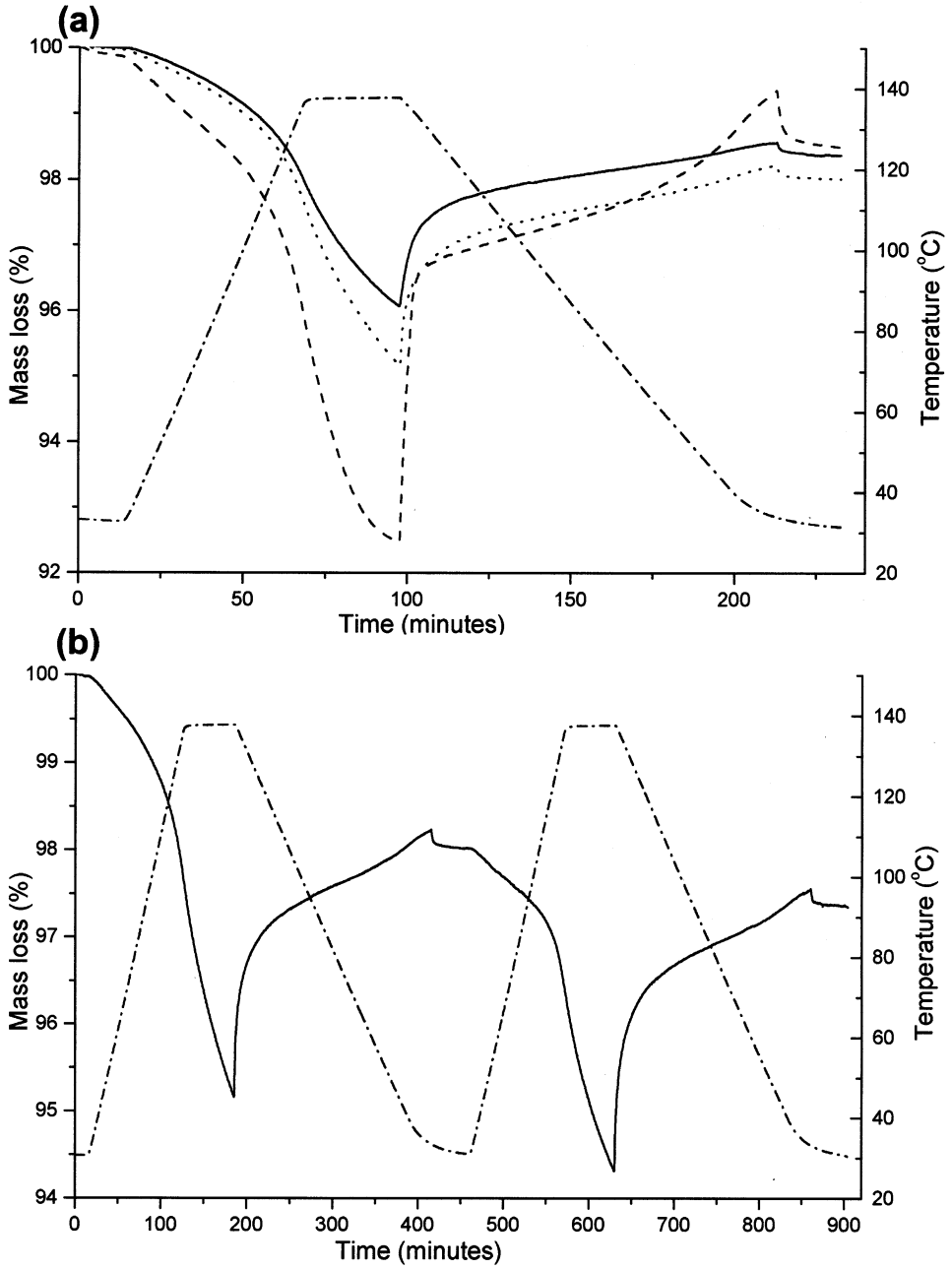

Figure 10. TGA plot showing the desorption−readsorption behavior of (a) $Al_2[(O_3PC_2H_4PO_3)_{1-x}(HPO_3)_{2x}](H_2O)_2F_2{\cdot}H_2O$ ($x = 0$ (solid), $x = 0.19$ (dots), and $x = 0.32$ (dashes)); and two cycles of desorption−readsorption behavior of (b) $Al_2[O_3PC_2H_4PO_3]_{0.810(5)}$-$[HPO_3]_{0.38(1)}(H_2O)_2F_2{\cdot}H_2O$. The temperature profiles are shown by the dot−dash lines in (a) and (b).

of bond lengths and angles, and values of $C(1)_{occ} = 0.803(5)$ and $C(1)_{Uiso} = 0.003(2)$ Å^2. This value of $C(1)_{occ}$ is in excellent agreement with that in Table 4 as we would expect, and the value of $C(1)_{Uiso}$ is much closer to that of the constrained $C(1)_{Uiso}$ value of 0.0091(4) Å^2 in Table 4. The formula of the phase $Al_2[(O_3PC_2H_4PO_3)_{0.810(5)}(HPO_3)_{0.38(1)}](H_2O)_2F_2{\cdot}H_2O$ obtained from the Rietveld analysis is in excellent agreement with the composition calculated from ^{31}P MAS SS NMR data, $Al_2[O_3PC_2H_4PO_3]_{0.81}[HPO_3]_{0.38}(H_2O)_2F_2{\cdot}H_2O$.

The structure of $Al_2[(O_3PC_2H_4PO_3)_{0.810(5)}(HPO_3)_{0.38(1)}]$-$(H_2O)_2F_2{\cdot}H_2O$ is shown in Figure 9, where it is seen that it adopts essentially the same framework structure as that described previously with all the bond lengths and angles (see Supporting Information) in reasonable agreement with those reported for $Al_2[O_3PC_2H_4PO_3](H_2O)_2F_2{\cdot}$ $0.51(3)H_2O$ (see Supporting Information). The major difference is that phosphite groups substitute 19.0% of the diphosphonate pillars, with each disphosphonate group being replaced by two phosphite groups as seen in Figure 9. The distance between adjacent diphosphonate groups is increased to 10.52 Å in the [010] direction, as seen in Figure 9a, and 9.57 Å in the [100] direction, as seen in Figure 9b, where the diphosphonate pillars are replaced. As the substitution of the diphosphonate groups is random, the formation of a larger pore running throughout the whole structure is unlikely to be present because this would require the phosphite groups to be incorporated into the material in an ordered manner. These crystallographic results indicate that the phosphite substitution leads to an increase in the overall porosity, or openness, of the material.

Readsorption Properties of the Phosphite/Diphosphonate Series: $Al_2[(O_3PC_2H_4PO_3)_{1-x}(HPO_3)_{2x}]$-

Table 5. Mass Changes of $Al[(O_3PC_2H_4PO_3)_{1-x}(HPO_3)_{2x}](H_2O)_2F_2{\cdot}H_2O$ Observed During the TGA Desorption−Readsorption Experiments

sample	mass loss (%)	mass gain (%)	readsorption (%)
$x = 0$	2.547	1.451	56.96
$x = 0.19$ 1st cycle	3.317	1.994	60.11
$x = 0.19$ 2nd cycle	2.686	2.091	77.86
$x = 0.32$	4.858	4.468	91.97

$(H_2O)_2F_2{\cdot}H_2O$ ($0 \leq x \leq 0.32$). As a final test to determine the success of the production of this phosphite/diphosphonate series, the porous nature of the series was probed by measuring their ability to reversibly desorb and adsorb their micropore contents. The water readsorption properties of the synthesized materials were probed using thermogravimetric analysis (TGA) following the procedure described in the Experimental Section. This heating scheme was selected as it results in a mass loss corresponding predominantly to that of the extraframework water molecule, O(6). Figure 10a shows the heating and cooling curves of the three samples, and Table 5 shows the magnitude of mass losses and gains associated with water desorption and readsorption. For all the samples in these experiments there is a low-temperature water loss (30−110 °C) which we attribute to loosely surface-bound water. It was assumed that the majority of the surface-bound water was removed as the sample reached 120 °C when the internal extraframework water starts to be removed, as seen in Figure 2 for a dry sample. The values of the mass changes presented in Table 5 were calculated from 120 °C to the conclusion of the 30-min dwell time at 135 °C for water desorption and the same temperature range, 135−120 °C, for the mass gain upon cooling attributable to the adsorption of extraframework water.

The mass change curves show that the temperature at which the extraframework water is first removed decreases in the order of increasing phosphite-substitution and that the amount of water lost and degree of readsorption, for this heating scheme, increases with the increasing quantity of phosphite substitution in the material. These observations are accounted for by considering the increase in porosity of the material upon increasing the degree of phosphite substitution. As more diphosphonate pillars are replaced by phosphite groups the internal volume of the material will become more open, allowing for easier diffusion of extraframework water molecules throughout the solid, and so resulting in desorption at lower temperatures and greater amounts of desorption and readsorption under these experimental conditions.

The heating and cooling cycles were repeated twice for the $x = 0.19$ substituted material in order to determine the recyclability of the water de-/readsorption. The results shown in Figure 10b, and values listed in Table 5, indicate that recycling of the sample with respect to reversible water adsorption is possible. A larger percentage readsorption occurs for the second cycle than the first which we assume to arise from residual surface-bound water in the calculations of the water desorbed in the first cycle that is not present in the second cycle.

Conclusions

This paper presents the first example of the successful use of the coprecipitation method with a trivalent metal cation phosphite/diphosphonate system to produce a solid solution series, $Al[(O_3PC_2H_4PO_3)_{1-x}(HPO_3)_{2x}](H_2O)_2F_2{\cdot}H_2O$, in which the porosity increases as the degree of phosphite substitution increases. The Rietveld refinement of the structure of the $x = 0.19$ member of the series reveals that this synthetic method yields a random distribution of phosphite groups throughout the bulk of the material and that the remainder of the framework of the material remains unaltered by incorporation of this moiety. The results show that for this type of material the coprecipitation technique can be used to synthesize crystalline products for which full Reitveld structure analysis can be performed. We also show that this coprecipitation technique can be used to control the degree of porosity within the material for the particular application that the material is intended. The incorporation of phosphite groups into other members of the group 13 diphosphonate family of materials is currently being investigated to determine the generality of the procedure as a synthetic step to create specific degrees of porosity within metal diphosphonate materials.

Acknowledgment. We thank Dr. A. Aliev (ULIRS), R. Jones (MSL, Daresbury Laboratory), Dr. S. J. Teat (SRS, Daresbury Laboratory), and Dr. E. J. Cussen (Department of Chemistry, University of Liverpool) for help in the collection of the ^{31}P NMR spectra, X-ray thermodiffraction data, single microcrystal X-ray diffraction data, and TGA data, respectively. We also thank Professors M. J. Rosseinsky (Department of Chemistry, University of Liverpool) and A. K. Cheetham (MRL, UCSB) for use of their TGA and NMR facilities, respectively. M.P.A. thanks the Royal Society for providing a University Research Fellowship, and H.G.H. thanks the EPSRC for provision of a quota award and for funding.

Supporting Information Available: The TGA, first derivative plot, and mass spectrometer readings for 20 amu (postulated to be HF), 15 amu (postulated to be CH_3), 26 amu (postulated to be C_2H_2), and 18 amu (postulated to be H_2O) for the heating of $Al_2[O_3PC_2H_4PO_3](H_2O)_2F_2{\cdot}H_2O$, the ^{31}P MAS SS NMR spectra of $Al_2[O_3PC_2H_4PO_3](H_2O)_2F_2{\cdot}H_2O$, tables of atomic coordinates, anisotropic thermal parameters, selected bond lengths and angles, and the CIF file for $Al_2[O_3PC_2H_4PO_3](H_2O)_2F_2{\cdot}0.51(3)H_2O$, and the table of selected bond lengths and angles for $Al_2[(O_3PC_2H_4PO_3)_{0.810(5)}(HPO_3)_{0.38(1)}](H_2O)_2F_2{\cdot}H_2O$. This material is available free of charge via the Internet at http://pubs.acs.org.

CM0212663